Study of the Optimum Injection Sites for a Multiple Metastases Region in Cancer Therapy by Using MFH

M. Pavel[1,2] and A. Stancu[1]

[1]Physics Department, Alexandru Ioan Cuza University, Iasi 700506, Romania
[2]Gr. T. Popa University of Medicine and Pharmacy, Iasi 700115, Romania

Metastases represent the final stage in cancer progression. Their early diagnosis and appropriate treatment are very important in order to maintain a high survival prognostic. The interest in MFH (Magnetic Fluid Hyperthermia) and cancer therapy has noticeably increased in the last years. There are still numerous problems that need to be solved before a clinical model may be tested. The goal of this paper is to both quantify the optimum dose of magnetic material and optimize injection sites in order to achieve a therapeutic temperature of 42°C that may induce apoptosis in tumor cells. A successful realization of this therapy implies a heating zone of at least 2 mm around the tumor. Finite Element Method (FEM) simulations of spherical metastases in liver and breast tissues near a blood vessel were performed using COMSOL Multiphysics (Heat Transfer Module) in order to simulate the temperature field produced by ferromagnetic nanoparticles within the tumor and healthy tissues. A systematical variation of tumor diameter and particle dosage was performed for every physical parameter for the tumor tissues mentioned above (e.g., tissue density, tumor/tissue perfusion rate) in order to understand the interdependence of these parameters and their effects on hyperthermia therapy.

Index Terms—**Bioheat equation, hyperthermia, magnetic nanoparticles, metastasis, perfusion rate.**

I. Introduction

CANCER cells often have aggressive tendencies to invade other areas of the body. Initially they group together to form a primary tumor. Once the tumor is formed, cells may begin to break off from this tumor and spread through the bloodstream or the lymph system [1], [2]. These cells metastasize to new organs, being capable of establishing new tumors in remote locations from the site of the original disease. Whether or not cancer cells metastasize (spread) to other parts of the body depends on many factors, including both the blood flow and the characteristics of the different cancer cells—the type and the stage of the cancer but also its original location [1]–[3].

Metastasis is the most common neoplasm in adult liver, and the liver is the second most common site for metastatic spread, after the lymph nodes. The liver may be the only organ involved in colorectal tumors and neuroendocrine tumors [1]. The most likely to metastasize to the liver, with a decreasing frequency, are colon, gastric, pancreas, breast and lung cancers [2]. An early detection of these metastasis, that is possible at the stage when they appear as micrometastases, and an appropriate treatment could increase the survival to 5 years and 10 years respectively. Metastases occur in the liver tissue usually close to blood vessels [3], [4].

Breast metastases are rarely present with patients mainly due to the first two filters present in the human organism: liver and lung. The most common types of cancers metastasizing in the breast tissue are malignant melanoma, cervical cancer, neuroendocrine-like tumors (in adults) and rhabdomyosarcoma (in children). These metastases are hard to differentiate histopathologically and mammographically from primary breast cancer [5]. Accurate diagnosis of breast metastasis could avoid unaesthetic mastectomy by implementing an appropriate systemic and local therapy.

A therapeutic realization of the metastasis cells' death also implies the involvement of a margin of healthy tissue. Although a margin limit of at least 10 mm has been recommended in literature [2], [3], a safe limit of 2 mm as a clinically acceptable minimum requirement has been proved in the case of micrometastases [6].

II. MFH Background

The new concept of inducing hyperthermia locally into the tumor was recognized as a promising form of cancer therapy among the classical methods such as chemotherapy, surgery and irradiation. This method is based on the principle that cancer cells growth may be stopped at temperatures higher than 42°C, while the normal cells may survive at even higher temperatures [7], [8].

The potential of the external alternating electromagnetic field effects in a nanoscale (characterized by a size of the magnetic nanoparticles less than 200–300 nm) was first described by Gordon *et al.* [9]. One of the most commonly used magnetic materials in hyperthermia cancer therapy by magnetic fluid is magnetite, Fe_3O_4 [7], [10]. The heating capabilities, magnetic properties, low toxicity and good biocompatibility of magnetite nanoparticles allow them to be used in different fields of biomedicine and biotechnology.

One of the focal points that have not yet been well understood and clarified for MFH is the control and generation of a well defined temperature area at the tumor. The goal is to quantify the optimum dose of magnetic material in order to achieve both a therapeutic temperature of at least 42°C inside the tumor and to limit the heating field to the tumor as precisely as possible.

When using magnetic nanoparticles, the heat generation within the tissue is attributed to two important loss processes [10]: hysteresis losses and relaxation losses which correspond to ferromagnetic regime (FM) and superparamagnetic regime (SPM) respectively. The loss power generated by hysteretic

Manuscript received March 06, 2009; revised May 15, 2009. Current version published September 18, 2009. Corresponding author: M. Pavel (e-mail: pmariana@stoner.phys.uaic.ro).

Color versions of one or more of the figures in this paper are available online at http://ieeexplore.ieee.org.

Digital Object Identifier 10.1109/TMAG.2009.2024543

processes is equal to the area of hysteretic loop multiplied by the frequency (f) of the alternating electromagnetic field [11]

$$\mathrm{LP_{FM}} = \mu_0 f \oint H dM \tag{1}$$

where permeability $\mu_0 = 4\pi \cdot 10^{-7}$ H/m.

The loss power (LP) given by the superparamagnetic regime is attributed to two major relaxation processes: Brownian and Néel relaxation, effects that are taken into account by considering the effective relaxation time, τ_R [8], [12]

$$\mathrm{LP_{SPM}} = \mu_0 \pi \chi_0 f \frac{2\pi f \tau_R}{1 + (2\pi f \tau_R)^2} H^2. \tag{2}$$

In (2) the magnetic susceptibility is given by $\chi_0 = \mu_0 M_S^2 V/(k_B T)$, where M_S is the saturation magnetization, V is the particle volume and $k_B = 1.38 \cdot 10^{-23}$ J/K.

In order to quantify the appropriate amount of LP generated by the magnetic nanoparticles, the field frequency (f) and field amplitude (H) must be carefully chosen. High values of field frequency and field amplitude may lead to lesions of the healthy tissues, reason for which some biocompatible criterions were established by Brezovich [13]. However, in order to successfully lead to the ablation of the whole tumor, Hergt [8] proposed a safe and tolerable criterion of exposure of $\mathrm{C} = 5 \times 10^9$ $\mathrm{Am^{-1}\ s^{-1}}$, where $\mathrm{H \cdot f} < \mathrm{C}$.

III. Computational Simulations of Heat Transfer in Biological Tissues

By taking into account both the biocompatibility criterion mentioned above and the useable range of frequency and amplitude proposed by Pankhurst [7], we concluded in a previous paper [14] that for particles that describe a hysteretic behavior the field amplitude and frequency values should be less than 15 kA/m and 500 kHz respectively. The loss power obtained in these conditions is less than 7.5×10^9 W/m^3, value that corresponds to field amplitude less than 7.0 kA/m and field frequency less than 200 kHz for considered particles of 18 nm in diameter—the case of superparamagnetic behavior. Although our work assumes a monodispersion of the nanoparticles, we have observed that these results are close to those obtained experimentally by Hergt [8], [10] or Pankhurst [7] in similar conditions (field frequency and amplitude) for polydisperse particle samples. We have also concluded the benefits of magnetite magnetic material and we advanced our simulations by taking into account the physical properties of magnetite.

Finite Element Method (FEM) simulations were performed using COMSOL Multiphysics (Heat Transfer Module) in order to simulate the heat dissipation by the magnetic nanoparticles into the cancer and normal tissues.

The transfer of thermal energy in living tissues is a complex process which involves both metabolic heat and blood flow. The blood perfusion rate through the vascular network on the local temperature distribution affects in different manners the bioheat transport into the body by interacting with other physiological processes such as thermoregulation or inflammation. The most commonly used equation that best describes the heat transfer within the tissue is Pennes' bioheat equation which describes both the effects of blood perfusion and the energy generated by the metabolic processes [15], [16]:

TABLE I
Physical and Physiological Properties

Type of Tissue	Density (kg/m^3)	Perfusion Rate (1/s)	Heat Capacity (J/kg·K)	Thermal conductivity (W/m·K)
Liver	1060[15]	0.0064[15]	3600[15]	0.512[15]
Colorectal Carcinoma	21500[18]	0.0064[15]	132[18]	0.71[18]
Breast Tumor	1060[18]	0.01333[17]	2300[19]	0.57[18]
Breast	980[19]	0.00667[19]	2300[19]	0.57[18]
Cervical Cancer	1160[18]	0.014[19]	132[18]	0.71[18]
Malignant Melanoma	1160[18]	0.0135[19]	1730[19]	0.512[18]

$$\delta_{\mathrm{tz}} \rho c \frac{\partial T}{\partial t} + \nabla \cdot (-k \nabla T) = \rho_b c_b \omega_b (T_b - T) + Q_{\mathrm{met}} + Q_{\mathrm{ext}} \tag{4}$$

where ρ is the tissue density, c is the tissue specific heat, ρ_b is the density of blood—1000 kg/m^3 as approximate value, c_b is the blood's specific heat—4180 J/(kg·K), k is the tissue thermal conductivity, ω_b is the blood perfusion rate, T_b is the arterial blood temperature, approximated as the core temperature of the body—310.15 K [15], [16], Q_{met} is the metabolic heat source, which for glandular tissue is 700 W/m^3 and for cancerous tissue is 5790 W/m^3 [17] and Q_{ext} is the heat generated by loss power.

For magnetite we considered the heat capacity of 670 J/(kg·K) and the density of 5180 kg/m^3. The physical and physiological properties of the analyzed tissues are presented in Table I.

We designed distinct simulations of a spherical tumor located in a 14 mm × 16 mm × 14 mm region from the tissue we intended to analyze (liver and breast tissues with their respective physical and physiological properties). The purpose of the models was to simulate the spatial temperature distribution within the tissue in order to understand the strong connections between the local and external factors involved in the MFH process. For therapeutic LP and magnetite concentration values we have chosen a range between $(3.6\text{–}7.6) \times 10^9$ W/m^3 and 8–12 mg/cm^3 of tumor tissue respectively.

For the first simulations we have computed the temperature field in the liver tissue when the metastases (MTS) were located next to a blood vessel (BV) with a radius of 0.5 mm, especially when we take into account the fact that they occur in the liver tissue, usually close to them (BVs). The two MTS with a diameter of 2.7 mm each are situated at 4.5 mm distance from the BV. The distance between the MTS is 1.3 mm and they are symmetrically placed from the y axis that passes through the BV's center.

For the first simulation the nanoparticles were randomly concentrated in 6 small spherical, each 0.9 mm in diameter, within each tumor region. Based on the idea that a therapeutic result implies a heating zone of at least 1.5–2 mm around the metastatic region, in the second simulation we concentrated the nanoparticles not only inside the tumor but also in the region between the two MTS. The nanoparticles are included in five small regions inside each tumor and one spherical region between the two MTS.

We firstly compared the results achieved from these two simulations and analyzed the temperature distribution inside the liver

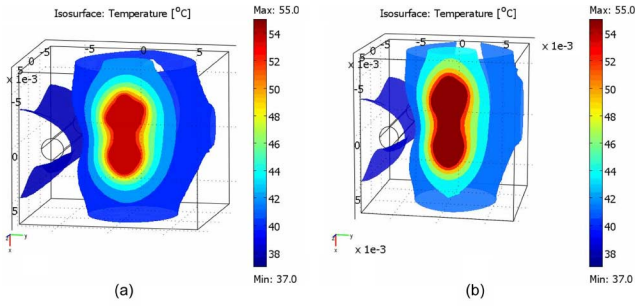

Fig. 1. Spatial temperature distribution in (a) liver MTS from colorectal carcinoma for a concentration of nanoparticles of 14 mg/cm^3 and (b) breast MTS from cervical cancer for a concentration of nanoparticles of 9 mg/cm^3 and LP value of 5.2×10^9 W/m^3.

tissue at different distances from both the MTS-complex region and each MTS center.

Secondly, we focused further on the blood constant systemic temperature's effect on the heat distribution into the tissue by increasing the BV's radius to 1 mm from the second simulation presented.

For our next simulation we have systematically varied the dimension of one of the two MTS from 2.7 up to 4.2 mm starting with latter model. The magnetite nanoparticles were placed in 6 small regions of 0.9 mm diameter inside the MTS larger than 3.8 mm. In the case of one MTS of 4.2 mm one extra small region with magnetic nanoparticles was included in the simulation, located in the space between the two MTS. We considered representative the cases with tumors having 3.3, 3.9 and 4.2 mm diameter respectively (see Fig. 1).

Based on the model with one MTS of 3.9 mm diameter, the distance between the two MTS was varied up to 2 mm (the necessary limit for a safe removal of tumor cells). The BV was further moved 1 mm on the negative y axis, the distance from the smallest MTS becoming almost 5.4 mm. These last simulations revealed the MFH cancer therapy outcome for metastases located nearer or further to each other and from a blood vessel respectively.

The temperature field in the breast tissue was also modeled following the already described simulation with the specificity of using the respective tissues' characteristics.

For both the liver and breast tissues the physical and physiological properties of two types of MTS were taken into account: liver metastasis from colorectal carcinoma and breast tumor and breast metastasis from malignant melanoma and cervical cancer.

IV. Results and Discussions

The first model describes the temperature field in the liver and breast tissue when the first two simulations are computed. Thus, we compared the results achieved from these two models and analyzed the temperature distribution inside the tissue at different distances from both de MTS complex region and each MTS region (one MTS $\text{diameter} = 2.7$ mm). The LP value was varied between $(3.4\text{–}5.2) \times 10^9$ W/m^3 for a concentration of magnetic nanoparticles ranging from 8 up to 15 mg/cm^3. We have discovered that for both liver and breast metastases closely located an optimum heating zone around the tumor region is obtained by spreading the nanoparticles not only inside them, but also in the tissue between them. Another remarkable aspect was the higher temperature value achieved at a minimum 1 mm

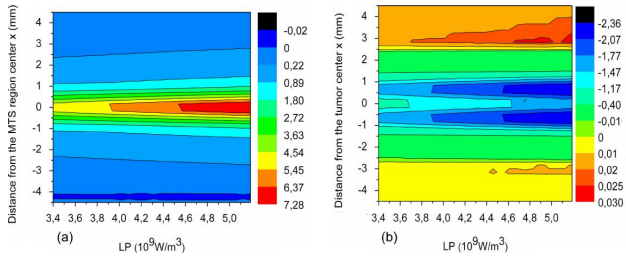

Fig. 2. Temperature differences (°C) in liver MTS from colorectal carcinoma when the first two models are used for a concentration of 12 mg/cm^3 at various distances from (a) the MTS-complex center (b) one MTS center.

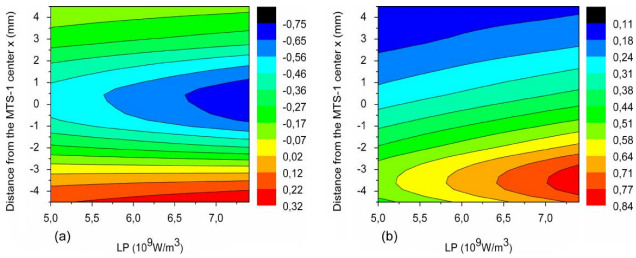

Fig. 3. Temperature differences (°C) in liver MTS from colorectal carcinoma for a concentration of 9.5 mg/cm^3 when (a) the two MTS are at a distance one from another of 2 mm and 1.3 mm respectively (b) the BV is at a distance of 5.4 mm and 4.5 mm respectively from the MTS.

outside the tumor region in the case with nanoparticles also injected in the space between the two MTS in comparison with the other one. The BV of 0.5 mm radius, located at 4.5 mm distance from each MTS, seems to have a slight influence on the heat dissipation.

In the second model the BV radius was enlarged from 0.5 mm up to 1 mm with the nanoparticles also spread outside the tumor region. The temperature decreases more in the case of the larger BV than in the initial one. It may be noticed a tendency for the difference between the spatial temperatures in the two cases to increase when the LP value is enlarged. The therapeutic temperature at 2 mm distance from the MTS is achieved for LP values higher than 5.0×10^9 W/m^3 and a concentration of nanoparticles larger than 11 mg/cm^3 of tumor volume. These observations are expressed in the Fig. 2 for the liver tissue.

By increasing the MTS diameter to 3.3 mm an optimal temperature at 2 mm distance is realized for a concentration of 13 mg/cm^3 and LP values of $(4.5\text{–}5.0) \times 10^9$ W/m^3. Decreasing concentration to 10 mg/cm^3 the LP values is increased to $(5.5\text{–}6.5) \times 10^9$ W/m^3. In the simulation with one of the two MTS of 4.2 mm diameter—the nanoparticles are concentrated in 13 spherical regions that are randomly distributed inside and outside of them, the successful outcome (a temperature ranging between 42–43°C) is achieved by using the following parameters: $\text{LP} = (3.8\text{–}4.8) \times 10^9$ W/m^3 corresponding to a concentration of nanoparticles of 13–13.5 mg/cm^3 and $\text{LP} = (5.8\text{–}6.8) \times 10^9$ W/m^3 for 8.5–9 mg/cm^3 respectively. The results presented correspond to liver metastases from colorectal carcinoma.

Fig. 3 describes the effect of a greater distance between the two MTS and the MTS complex region and BV respectively with the heat dissipation within the tissues. Distances comparable to the MTS dimensions do not considerably affect the temperature at 1.5–2 mm around the tumor border. Another reason to consider its importance in the MFH efficiency is that the temperatures for the BV on the tumors side are greater than on the

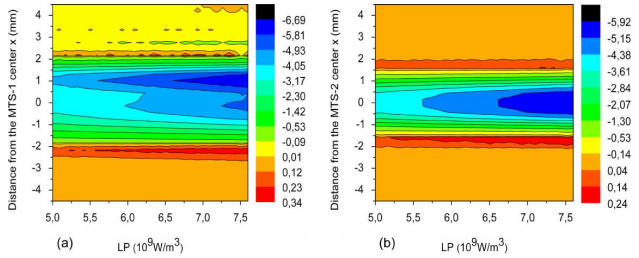

Fig. 4. Comparison between temperature differences (°C) for the breast MTS from cervical cancer and malignant melanoma at a concentration of 9.5 mg/cm^3 (a) MTS-1 diameter = 3.9 mm (b) MTS-2 diameter = 2.7 mm.

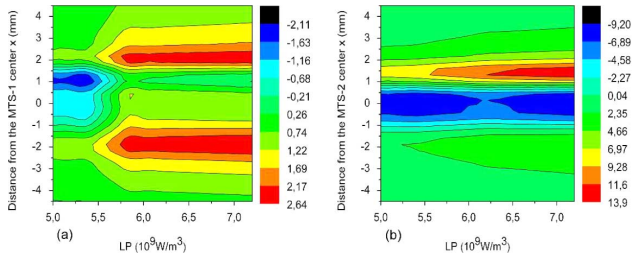

Fig. 5. Comparison between temperature differences (°C) for the liver MTS from colorectal carcinoma and breast tumor at a concentration of 11.5 mg/cm^3 (a) MTS-1 diameter = 3.9 mm (b) MTS-2 diameter = 2.7 mm.

other side [Fig. 3(a)]. The BV movement with 1 mm seems to have a noticeable influence in increasing the temperature field within the tissues [Fig. 3(b)].

Therapeutic parameters for breast metastases of MTS-1 (diameter = 3.9 mm) and MTS-2 (diameter = 2.7 mm) (see Fig. 4) are: LP = (6.8–7.5) × 10^9 W/m^3 for concentration = 10.0–10.5 mg/cm^3 and LP = (5.0–5.8)×10^9 W/m^3 for concentration = 14.0–14.5 mg/cm^3. The differences in spatial temperature distribution are better observed inside the MTS volume than at 2 mm away from it. This effect is explained by the similar values for tumor densities and perfusion rates.

The high temperature differences may be explained by considering the physical and physiological properties of liver metastases from colorectal carcinoma and breast tumor (especially tumor density and perfusion rate) (see Fig. 5).

Moreover these variations decrease with larger tumors, this being more obvious with very small metastases (less than 2.7–3 mm). The temperature differences inside the two types of MTS decrease by increasing the LP value (field frequency and amplitude).

In all our computational simulations we assumed a monodispersion of nanoparticles. The size polydispersity, which is present in all real nanoparticle samples, has a decreasing influence on the loss power that can be achieved [20]. By using highly monodisperse samples of 18 nm diameter, the heating rate variation is better limited [20], but the intrinsic carrier fluid parameters such as specific heat, mass density and viscosity influence the expected outcome. We are interested in a further systematical analysis of the degradative influence of polydispersity.

V. Conclusion

One of the focal points of MFH, the choice of the right dose of nanoparticles and the applied field parameters in order to achieve the optimal temperature for a given patient with a well described condition is still uncertain. Nevertheless, if the micrometastasis shape and position are known from suitable suitable medical imaging techniques (e.g., MRI, CT) and by using these models it is possible to estimate the impact of the particle dose on the efficiency of hyperthermia therapy, also taking into account the local features (e.g., tumor density, type and perfusion rate, blood vessels of large size close located) and external factors (e.g., field amplitude and frequency) involved.

Acknowledgment

This work was supported in part by the Romanian PNII-26 NANOPART project.

References

[1] P. J. Robinson, "Imaging liver metastases: Current limitations and future prospects," *Br. J. Radiol.*, vol. 73, pp. 234–241, 2000.
[2] J. Scheele, R. Stangl, and A. Altendorf-Hofmann, "Hepatic metastases from colorectal carcinoma: Impact of surgical resection on the natural history," *Br. J. Surg.*, vol. 77, pp. 1241–1246, 1990.
[3] B. Cady *et al.*, "Technical and biological factors in diseasefree survival after hepatic resection for colorectal cancer metastases," *Arch. Surg.*, vol. 127, pp. 561–569, 1992.
[4] J. Hohmann, T. Albrecht, A. Oldenburg, J. Skrok, and K.-J. Wolf, "Liver metastases in cancer: Detection with contrast-enhanced ultrasonography," *Abdom. Imag.*, vol. 29, pp. 669–681, 2004.
[5] B. Vergier, M. Trojani, I. De Mascarel, J. M. Coindre, and A. Le Treut, "Metastases to the breast: Differential diagnosis from primary breast carcinoma," *J. Surg. Oncol.*, vol. 48, no. 2, pp. 112–6, 1991.
[6] N. Kokudo *et al.*, "Genetic and histological assessment of surgical margins in resected liver metastases from colorectal carcinoma: Minimum surgical margins for successful resection," *Arch. Surg.*, vol. 137, pp. 833–40, 2002.
[7] Q. A. Pankhurst, J. Connolly, S. K. Jones, and J. Dobson, "Applications of magnetic nanoparticles in biomedicine," *J. Phys. D: Appl. Phys.*, vol. 36, pp. R167–R181, 2003.
[8] R. Hergt and S. Dutz, "Magnetic particle hyperthermia-biophysical limitations of a visionary tumour therapy," *J. Magn. Magn. Mater.*, vol. 311, pp. 187–192, 2007.
[9] R. T. Gordon and J. R. Hines, "Intracellular hyperthermia: A biophysical approach to cancer treatment via intracellular temperature and biophysical alterations," *Med. Hypotheses*, vol. 5, p. 83, 1979.
[10] R. Hergt, W. Andra, C. G. D'Ambly, I. Hilger, W. A. Kaiser, U. Richter, and H. G. Schmidt, "Physical limits of hyperthermia using magnetite fine particles," *IEEE Trans. Magn.*, vol. 34, no. 6, pp. 3745–3754, Dec. 1998.
[11] S. Bae, S. W. Lee, Y. Takemura, E. Yamashita, J. Kunisaki, S. Zurn, and C. S. Kim, "Dependence of frequency and magnetic field on self-heating characteristic of NiFe2O4 nanoparticles for hyperthermia," *IEEE Trans. Magn.*, vol. 42, pp. 3566–3568, 2006.
[12] B. Payet, A. Siblini, M. F. Blanc-Mignon, and G. Noyel, "Comparison between a magneto-optical method and Fannin's technique for the measurement of Brown's relaxation frequency of ferrofluid," *IEEE Trans. Magn.*, vol. 35, pp. 2018–2023, 1999.
[13] I. A. Brezovich and R. F. Meredith, "Practical aspects of ferromagnetic thermoseed hyperthermia," *Radiol. Clin. North. Am.*, vol. 27, pp. 589–602, 1989.
[14] M. Pavel, G. Gradinariu, and A. Stancu, "Study of the the optimum dose of ferromagnetic nanoparticles suitable for cancer therapy using MFH," *IEEE Trans. Magn*, vol. 44, Nov. 2008.
[15] COMSOL Multiphysics, Heat Transfer Module, User's Guide pp. 145–161 and Model Library, pp. 243–264.
[16] H. H. Pennes, *J. Appl. Physiol.*, vol. 1, pp. 93–, 1984.
[17] E. Y. K. Ng and N. M. Sudharsan, "Effect of blood flow, tumour and cold stress in a female breast: A novel time-accurate computer simulation," *J. Biomed. Eng.*, vol. 215, pp. 393–404, 2001.
[18] C. B. Saw, A. Loper, K. Komanduri, T. Combine, S. F. Huq, and C. Scicutella, "Determination of CT-to-density conversion relationship for image-based treatment planning systems," *Med. Dosim.*, vol. 30, pp. 145–148, 2005.
[19] C. Sturesson and S. A. Engels, "A mathematical model for predicting the temperature distribution in laser-induced hyperthermia. Experimental evaluation and applications," *Phys. Med. Biol.*, vol. 40, pp. 2037–2052S, 1995.
[20] R. E. Rosensweig, "Heating magnetic fluid with alternating magnetic field," *J. Magn. Magn. Mater.*, vol. 252, pp. 370–374, 2002.